



1 **Vertical characterization of Highly Oxygenated Molecules**
2 **(HOMs) below and above a boreal forest canopy**

3

4 Qiaozhi Zha¹, Chao Yan¹, Heikki Junninen¹, Matthieu Riva¹, Juho Aalto¹, Lauriane
5 Quéléver¹, Simon Schallhart¹, Lubna Dada¹, Liine Heikkinen¹, Otso Peräkylä¹, Jun
6 Zou², Clémence Rose¹, Yonghong Wang¹, Ivan Mammarella³, Gabriel Katul^{4,5}, Timo
7 Vesala¹, Douglas R. Worsnop^{1,6}, Markku Kulmala¹, Tuukka. Petäjä¹, Federico
8 Bianchi¹, and Mikael Ehn¹

9

10 ¹ Department of Physics, University of Helsinki, P.O. Box 64, 00014 Finland

11 ² CMA-NJU Joint Laboratory for Climate Prediction Studies, Institute for Climate and
12 Global Change Research, School of Atmospheric Sciences, Nanjing University,
13 Nanjing, China

14 ³ Department of Physics, University of Helsinki, P.O. Box 48, 00014 Finland

15 ⁴ Nicholas School of the Environment, Duke University, Durham, North Carolina, USA

16 ⁵ Department of Civil and Environmental Engineering, Duke University, Durham,
17 North Carolina, USA

18 ⁶ Aerodyne Research, Inc., Billerica, MA 01821, USA

19 Correspondence to: Qiaozhi Zha (qiaozhi.zha@helsinki.fi) and Chao Yan (chao.yan@helsinki.fi)

20

21 **1 Abstract**

22 While the role of highly oxygenated molecules (HOMs) in new particle formation (NPF)
23 and secondary organic aerosol (SOA) formation is not in dispute, the interplay between
24 HOM chemistry and atmospheric conditions continues to draw significant research
25 attention. During the Influence of Biosphere-Atmosphere Interactions on the Reactive
26 Nitrogen budget (IBAIRN) campaign, profile measurements of neutral HOM molecules
27 below and above the forest canopy were performed for the first time in the boreal forest
28 SMEAR II station during September 2016. The HOM concentrations and composition
29 distributions below and above the canopy were similar, supporting a well-mixed
30 boundary layer approximation during daytime. However, much lower HOM



31 concentration were frequently observed at ground level due to the formation of a
32 shallow decoupled layer below the canopy attached to the forest floor. Near ground
33 HOMs were influenced by the changes in the precursors and oxidants, and enhancement
34 of the loss on surfaces in this layer, while the HOMs above the canopy top were not
35 significantly affected. Our findings also illustrate that near-ground HOM measurements
36 conducted in strong stably stratified conditions might only be representative of a small
37 fraction of the entire nocturnal boundary layer. This might, in turn, influence the growth
38 of newly formed particles and SOA formation below the canopy where a large majority
39 of measurements are typically conducted.

40 **2 Introduction**

41 Highly oxygenated molecules (HOMs), a sub-group of the oxidation products of
42 volatile organic compounds (VOCs) identified by their high oxidation states, have been
43 recognized as important precursors for organic aerosol in the atmosphere (Ehn et al.,
44 2014). They have also been found to enhance new particle formation (NPF) and growth
45 (Kulmala et al., 2013; Zhao et al., 2013; Ehn et al., 2014; Bianchi et al., 2016; Kirkby
46 et al., 2016; Tröstl et al., 2016). The importance of HOMs has been confirmed in
47 ambient environments, especially in monoterpene-dominated regions such as the boreal
48 forest (Kulmala et al., 2013; Ehn et al., 2014), but also in high altitude mountain regions
49 (Bianchi et al., 2016) and in rural areas (Jokinen et al., 2014a; Kürten et al., 2016). In
50 laboratory studies, HOM formation has been observed from various precursor
51 molecules (Ehn et al., 2017), including both biogenic and anthropogenic emissions.

52

53 The direct observation of HOMs has only recently become possible, following the
54 developments of the Atmospheric-Pressure-interface Time-Of-Flight (APi-TOF,
55 measures the charged HOM clusters) (Junninen et al., 2010) and Chemical Ionization
56 Atmospheric-Pressure-interface Time-Of-Flight (CI-APi-TOF, measures the neutral
57 HOM molecules) (Jokinen et al., 2012) mass spectrometers. Ehn et al. (2010) and



58 Bianchi et al. (2017) found that the naturally charged HOM clusters could be observed
59 every night in boreal forest during spring. Out of the observed ambient mass spectra, a
60 significant part could be reproduced in a chamber by introducing the monoterpene α -
61 pinene ($C_{10}H_{16}$, the major biogenic VOC in the boreal forest) and ozone (O_3) (Ehn et
62 al., 2012).

63
64 Further investigations of HOM formation chemistry have been done in both laboratory
65 and field studies. Based on current understanding from laboratory experiments, the
66 formation of HOM molecules involves three main steps: 1) initial formation of peroxy
67 radicals (RO_2) from VOC oxidation; 2) RO_2 auto-oxidation, that is, the isomerization of
68 the RO_2 via intramolecular H-shifts and the subsequent oxygen (O_2) additions; and 3)
69 radical termination, forming closed-shell molecules (Crouse et al., 2013; Ehn et al.,
70 2014; Jokinen et al., 2014b, 2016; Rissanen et al., 2014; Mentel et al., 2015). In the
71 atmosphere, HOM formation studies are complicated by the plethora of different
72 compounds and processes taking place. However, recent ambient measurements
73 together with factor analysis were able to shed light on the HOM formation pathways
74 in the boreal forest (Yan et al., 2016). They showed that the majority of the daytime
75 production of HOMs was from reactions initiated by the oxidation of monoterpenes
76 (MT) with hydroxyl radical (OH) or O_3 . The RO_2 after auto-oxidation was either
77 terminated by hydroperoxyl radical (HO_2) or self-termination (Orlando and Tyndall,
78 2012), to form a non-nitrate HOM monomer ($CHO_{monomer}$, mainly C_9 and C_{10}
79 compounds, masses between 290-450 Th after clustering with the charging ion (NO_3^-)
80 of the instrument); or reacting with nitrogen oxides (NO_x) to form an organonitrate
81 HOM monomer ($CHON_{monomer}$). During nighttime, MT were mainly oxidized by O_3
82 and NO_3 radical. Furthermore, due to the lower nocturnal HO_2 and NO_x concentrations,
83 besides the production of $CHON_{monomer}$, the RO_2 products could also react with another
84 RO_2 to form a non-nitrate HOM dimer (CHO_{dimer} , mainly C_{16-20} compounds, masses
85 between 450-600 Th after clustering with NO_3^-) or an organonitrate HOM dimer



86 (CHON_{dimer}), depending on the oxidants of the RO₂ radical. (Ehn et al., 2014; Yan et
87 al., 2016).

88

89 Beyond those chemical pathways, varied meteorological conditions are also factors
90 influencing the MT and oxidants at different heights above the forest floor.
91 Unsurprisingly, the oxidants of HOMs (e.g. O₃) were found almost uniformly
92 distributed within the well-mixed daytime boundary layer (Chen et al., 2017). In
93 contrast, the nocturnal boundary layer was shallow with stability regimes that depended
94 on radiative cooling within the canopy and turbulent shear stresses at the canopy top.
95 In Hyytiälä, the depletions of O₃ in the sub-canopy level were frequently observed
96 during nighttime, while the O₃ above the canopy was less affected. The MT
97 concentration at ground level increased when O₃ was depleted (Eerdekens et al., 2009).
98 The inhomogeneous distribution of the precursors and oxidants below and above the
99 canopy might further impact nocturnal HOM distributions, which frames the scope of
100 this study. Until now, all CI-API-TOF deployments have been at ground level, and the
101 main subject of inquiry here is the vertical information on HOMs and the role of
102 meteorological condition in shaping them. A characterization of the HOMs at different
103 heights provides a decisive advantage in disentangling the role of non-uniform mixing
104 within the atmospheric layers impacted by strong thermal stratification, especially
105 inside the canopy volume.

106

107 The first measurements of the HOM concentrations at two different heights (36 m and
108 1.5 m a.g.l.) during September 2016 are presented and discussed. The influence of
109 boundary layer dynamics on the HOMs at these different heights are explicitly analyzed
110 and characterized in conjunction with auxiliary turbulence and micrometeorological
111 measurements.



112 **3 Experimental**

113 **3.1 Measurement site description**

114 The measurements were performed at the SMEAR II station (Station for Measuring
115 Ecosystem–Atmosphere Relations) in the boreal forest in Hyytiälä, southern Finland
116 (61°51' N, 24°17' E, 181 m a.s.l., Hari and Kulmala, 2005; Hari et al., 2013) during
117 September 2016. There is no large anthropogenic emission source at or near the site.
118 The closest sources are the two sawmills ~5 km southeast from the site and emission
119 from the city area of Tampere (~60 km away). The forest surrounding the station is
120 primarily Scots pine with a mean canopy height of ~17.5 m (Bäck et al., 2012). The
121 planetary boundary layer height at the SMEAR II station has been determined from
122 previous studies using radiosondes (Lauros et al., 2007; Ouwersloot et al., 2012) and
123 balloon soundings (Eerdeken et al., 2009). Roughly, these heights span some 400 m
124 (March) to 1700 m (August) at noontime, and 100 m (March) to <160 m (April) at
125 midnight.

126 **3.2 Instrumentation**

127 Concentration of HOM molecules were measured with two nitrate-ion based CI-APi-
128 TOF mass spectrometers. The CI-APi-TOF measuring at higher altitude was deployed
129 to the top of a 35 m tower located ~20 m horizontally from the ground measurement
130 location. The inlets of the two instruments were pointed to the southeast direction and
131 fixed at ~36 m and ~1 m above ground. The tower measurement is about twice the
132 canopy height, which is still within the roughness sublayer of the forest (Raupach and
133 Thom, 1981). The instrument setup of the two CI-APi-TOF mass spectrometers were
134 similar. In brief, the CI-APi-TOF was the combination of a chemical ionization (CI)
135 inlet, and an atmospheric pressure interface time-of-flight (APi-TOF) mass
136 spectrometer (Aerodyne Research Inc., USA, and Tofwerk AG, Switzerland). The
137 ambient air was first drawn into the inlet with a sample flow of 7 lpm (liter per minute),



138 and then converged to the center of an ion reaction tube surrounded by sheath flow
139 (filtered air, 35 lpm). Meanwhile, the nitrate ions carried by the sheath gas, which were
140 generated by exposing the nitric acid (HNO_3) to soft x-ray radiation, were guided into
141 the sample gas by an electrical field at ambient pressure (~ 100 ms reaction time).
142 Neutral molecules (M) in the sample air were ionized by either clustering with charged
143 nitrate/nitric acid ($(\text{HNO}_3)_{n=0.2}\cdot\text{NO}_3^-$) to form $(M)\cdot\text{NO}_3^-$ cluster ions, or losing a proton
144 to the charging ions to form deprotonated ions (e.g., $\text{H}_2\text{SO}_4 + \text{NO}_3^- \rightarrow \text{HSO}_4^- + \text{HNO}_3$).
145 The ions then entered the APi part, which was a three-stage vacuum chamber, through
146 a pinhole. In the APi, two quadrupoles and a stack of ion lenses guide the ions into the
147 TOF mass spectrometer, where ions were separated based on their mass-to-charge (m/z)
148 ratios. A more detailed description of this instrument has been given by Junninen et al.
149 (2010) and Jokinen et al. (2012). Mass spectra obtained from the instrument were
150 analyzed using the 'tofTools' program described in Junninen et al. (2010).
151 Determination of the concentration of a measured molecule M was based on the
152 following equation:

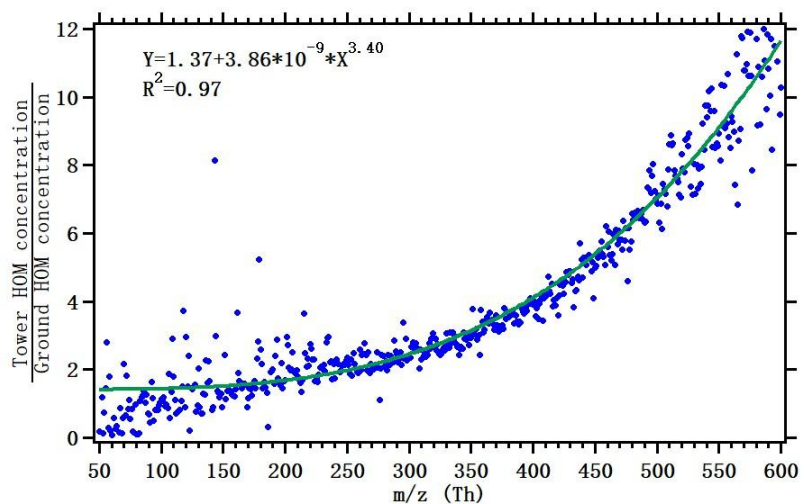
$$153 \quad [M] = \frac{M}{\sum \text{reagent ion count rates}} \times C \quad (1)$$

154 where the sum of ion count rates was an inclusion of all detected ions relating to
155 compound M , whether deprotonated or in clusters with reagent ions, and the sum of
156 reagent ion count rates is the total signal of the charged nitric acid ions. C was the
157 calibration coefficient, which was assigned the same value for all detected compounds.
158 This assignment is only valid for compounds that cluster with the reagent ions at the
159 collision limit, such as H_2SO_4 (Viggiano et al., 1997) and have equal collision rates.
160 The collision rates of nitrate ions with H_2SO_4 and with HOMs are expected to be very
161 close (Ehn et al., 2014). Here, a calibration coefficient of 1×10^{10} molec cm^{-3} , estimated
162 from previous calibrations with similar settings using sulfuric acid and theoretical
163 constraints (Ehn et al., 2014), with an uncertainty of $-50\%/+100\%$, was used in
164 calculating the HOM concentrations for both instruments. Ultimately, the absolute
165 HOM concentrations in this work are of secondary importance, as we focus on the



166 relative comparison of HOM concentrations measured at different heights. However,
167 the comparability of the two CI-APi-TOF instruments is of great importance, and
168 results cannot be allowed to vary e.g. as a result of inevitable differences in the mass-
169 dependent transmission efficiency (TE). To this end, instead of directly evaluating the
170 TE of each instrument, a “relative” TE of the two CI-APi-TOFs was used for data
171 correction: we selected a time period at noon-time on September 9 with well-mixed
172 boundary layer condition, identified with the clear and sunny weather and
173 homogeneous vertical distribution of monoterpene and other trace gases, and assumed
174 the HOM concentrations at the two heights to be the same. Thus, the relative TE was
175 obtained from the concentration ratio between the two CI-APi-TOFs at each m/z (Figure
176 1). Weaker correlation was obtained in the sub-150 Th mass range, but in the mass range
177 where most of the HOMs were located (290-600 Th) there is very little scatter around
178 the fitted curve, clearly suggesting that observed differences in the two instruments
179 responses were mainly due to differences in TE. Additionally, an inter-comparison
180 between the two instruments with a permeation tube was conducted after the campaign,
181 and the results showed good agreement with the relative TE, lending confidence to the
182 method used here. Finally, it should be noted that the difference in TE between the two
183 instruments was larger than one would normally expect, since the tower CI-APi-TOF
184 had been tuned for maximum sensitivity at the largest masses (at the expense of
185 transmission at the lower masses).

186



187

188 Figure 1 The relative TE curve between the two CI-API-TOFs for data correction.

189

190 In comparison to the direct determination of TE (Heinritzi et al., 2016), this method
191 increases the uncertainty in the quantification of HOM concentrations. However, as
192 mentioned, a more accurate knowledge of the exact HOM concentrations would not
193 influence the main findings of this study.

194

195 The MT, trace gases, and meteorological parameters were continuously monitored at
196 the different heights (4.2 m, 8.4 m, 16.8 m, 33.6 m, 50.4 m, 67.2 m, 125 m) on a 126 m
197 mast ~100 m away from the location of the CI-API-TOFs. The data at 4.2 m and 33.6
198 m were used in this study to represent the concentrations at near ground and tower level,
199 respectively. Ambient MT concentration was measured every third hour using a proton
200 transfer reaction mass spectrometer with the lowest detection limit of 1 pptv (PTR-MS,
201 Ionicon Analytik GmbH; Taipale et al., 2008). The O₃ concentration was measured with
202 an UV light absorption analyzer that had a lowest detection limit of 1 ppbv (TEI model
203 49C, Thermo Fisher Scientific, USA). The NO_x measurement was conducted using a
204 chemiluminescence analyzer (TEI model 42C TL, Thermo Fisher Scientific, USA). The
205 lowest detection limit of the NO_x analyzer is 50 pptv. The CO₂ measurement was



206 performed using an infrared light absorption analyzer (URAS4 CO₂, Hartmann &
207 Braun, Germany). The aerosol number concentration size distributions were obtained
208 with a twin differential mobility particle sizer (twin-DMPS) for the size range from 3-
209 1000 nm (Aalto et al., 2001) at 8 m height above ground, and was used to calculate
210 condensation sink (CS) based on the method from Kulmala et al. (2001). Air
211 temperature was measured with PT-100 resistance thermometers. Air relative humidity
212 (RH) was measured with RH sensors (Rotronic Hygromet model MP102H with
213 Hygroclip HC2-S3, Rotronic AG, Switzerland). Global radiation (solar radiation in
214 wavelength range of 0.3-4.8 μm) was obtained with a Pyranometer (Reemann TP3,
215 Astrodata, Estonia) above the canopy top at 18 m. All the data presented are at 10 min
216 averaging interval except for the MT (in 1-hour averaging interval).

217

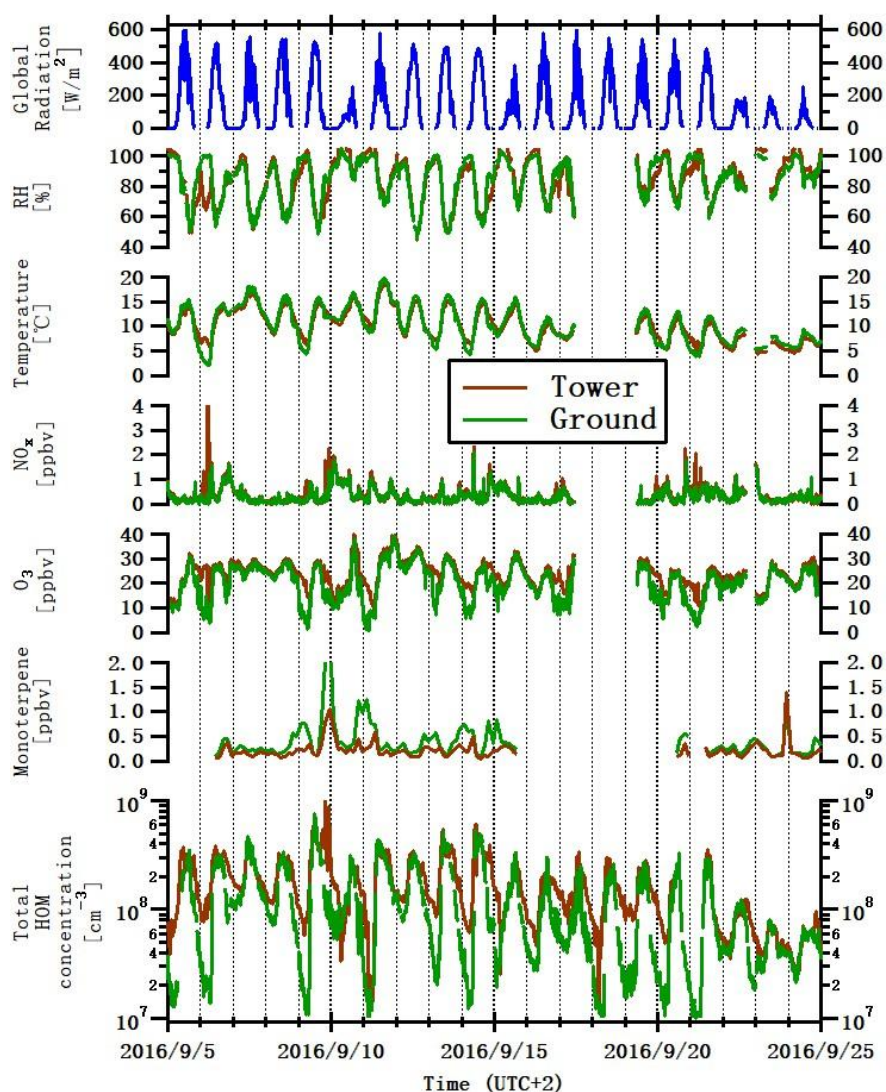
218 4 Results and discussion

219 4.1 Data overview

220 The Influence of Biosphere-Atmosphere Interactions on the Reactive Nitrogen budget
221 (IBAIRN) campaign was conducted from September 1 to 25, 2016. After data quality
222 checks, only the measurements collected after September 5 were used. Figure 2 shows
223 the overall time series of the meteorological parameters measured at ground and tower
224 levels, including the temperature, RH, global radiation, concentrations of trace gases,
225 MT, and total HOMs. The weather was generally sunny and clear during the campaign
226 except for a few cloudy (September 10, 15, and 22-23) and drizzling (September 24
227 and 25) days. The mean air temperature and RH of 10.8 ± 3.3 °C and $87.3 \pm 13.4\%$ (1σ
228 standard deviation) were observed at ground level, and 10.5 ± 3.0 °C and 88.2 ± 14.4 %
229 at tower level. The O₃ concentrations measured at ground and tower levels were $21.2 \pm$
230 7.6 ppbv and 24.9 ± 6.0 ppbv, respectively. The air temperature, RH and O₃ measured
231 at the two heights were close to each other during daytime. The NO_x concentrations
232 were quite low throughout the campaign, the mean NO_x concentrations were mostly



233 around the reported detection limit at 0.38 ± 0.35 ppbv (ground) and 0.44 ± 0.45 ppbv
234 (tower), yet showed an overall good agreement between the measurements at the
235 different heights. The MT concentrations at ground level (0.38 ± 0.34 ppbv on average)
236 was generally higher than that above the canopy level (0.20 ± 0.16 ppbv).
237



238
239 Figure 2 The overall time series of the measured trace gases, meteorological parameters and total HOM
240 concentrations at the ground (green) and tower (brown) levels.



241

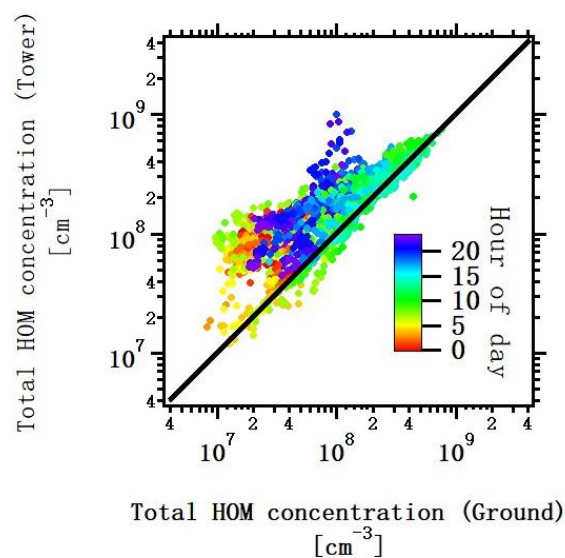
242 The total HOM concentration is representative for the overall concentration level of
243 HOMs, and is defined as the sum of the detected signals between ions from m/z 200 to
244 600 after removing the identified background peaks. The gaps in the ground total HOM
245 data were due to automatic zero-check. During the campaign, a significant difference
246 was found in the total HOM concentrations below and above the canopy (mean and
247 median concentrations of $1.1 \pm 1.7 \times 10^8 \text{ cm}^{-3}$ and $7.6 \times 10^7 \text{ cm}^{-3}$ at ground level, $1.7 \pm$
248 $1.3 \times 10^8 \text{ cm}^{-3}$ and $1.3 \times 10^8 \text{ cm}^{-3}$ at tower level). The causes of these differences frame
249 the upcoming discussion.

250

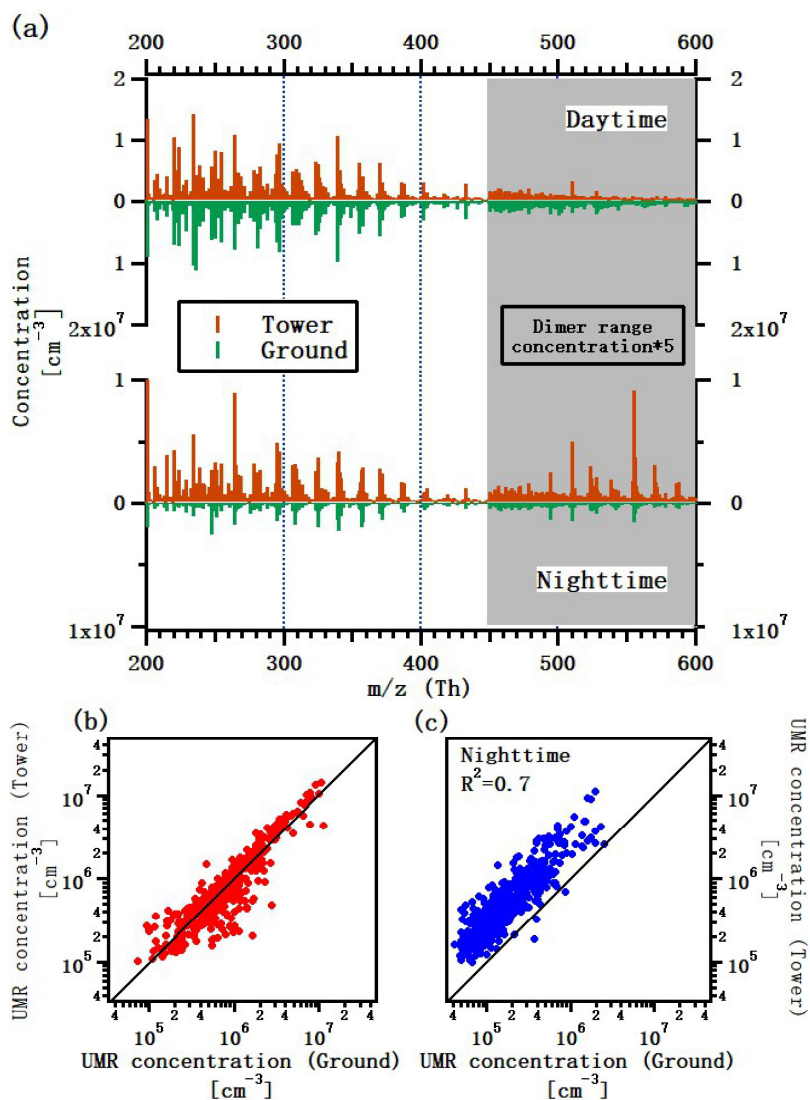
251 **4.2 Inter-comparison of total HOM concentrations**

252 The total HOM concentrations at the two heights were not different during the day,
253 which validates the use of only one day of data for scaling the TE of the ground CI-
254 APi-TOF to match the HOM signals. The good daytime agreement throughout the
255 campaign period also verifies that the response of each instrument stayed stable.
256 Contrary to the daytime results, the total HOM concentration at ground level usually
257 diverged from the tower measurement in the nocturnal boundary layer. The
258 concentration below the canopy became even lower when temperature inversions were
259 observed, accompanied by a decreasing ground-level O_3 and increasing MT
260 concentrations. Figure 3 shows the correlation between the total HOM concentrations
261 observed at two heights. Herein, good agreement could be found for the group of points
262 representing the concentrations around noontime. The points indicating the nighttime
263 total HOM concentrations were scattered, and the ground concentrations were found to
264 be much lower than the tower ones.

265



266
267 Figure 3 Correlation between ground (x-axis) and tower (y-axis) measurements of the total HOM
268 concentrations. The black line denotes the 1:1 ratio. Color code indicates the sampling time of HOMs.
269
270 Figure 4a shows the mean spectra (in unit mass resolution, UMR, between m/z 200 –
271 600) obtained from the ground and tower HOM measurements. It is worth mentioning
272 that there might be some signals not attributable to HOMs in the plotted spectra, but
273 only in little proportion. Only selected periods (09:00-15:00 for daytime and 21:00-
274 03:00 for nighttime, local winter time (UTC +2)) are included in the averaging period
275 to eliminate the effect of sunrise and sunset periods. During daytime, a good agreement
276 ($R^2 = 0.87$) was obtained from the mass-by-mass comparison (shown in Figure 4b)
277 using the UMR concentrations extracted from daytime mean spectra, suggesting a
278 uniform composition distribution in the daytime boundary layer condition. During
279 nighttime, the mean concentrations of all HOM molecules in the ground mean spectra
280 were much lower than the tower spectra. The HOM concentrations shown in the ground
281 and tower mean spectra were also less correlated in Figure 4c. Therefore, a logical
282 outcome is that the conditions below and above the canopy are experiencing different
283 turbulent mixing strength or source-sink regimes during night.
284



285

286 Figure 4 (a) Mean mass spectra with the averaging periods of daytime (09:00-15:00) and nighttime

287 (21:00-03:00) at ground and tower levels; (b) mass-by-mass comparison between ground and tower

288 UMR concentrations extracted from daytime mean spectra in Figure 4a; (c) mass-by-mass comparison

289 between ground and tower UMR concentrations extracted from nighttime mean spectra in Figure 4a.



290 **4.3 Influence of nocturnal boundary layer dynamics and micrometeorological**
291 **processes**

292 The nighttime HOMs at ground level are influenced by transport processes below the
293 canopy, since the total HOM concentrations were found much lower in the nights when
294 temperature inversions were observed. To further investigate the potential impact from
295 such micrometeorological phenomena on the ground HOMs, all the nights during the
296 campaign, after ruling out those with precipitation and instrument failures, were
297 selected (12 nights in total) and categorized into 2 types based on the appearance of the
298 temperature inversion: 1) the “non-inversion night” type included 6 nights when no
299 temperature inversion was recorded; 2) the “inversion night” type contained 6 nights
300 that had encountered temperature inversions, and the ground temperatures were
301 generally ~ 1 °C lower compared to tower temperatures during these nights.

302

303 **4.3.1 Statistics of the “non-inversion night” and “inversion night” types**

304 Table 1 shows the overall statistics including the mean, median, 25% percentile and 75%
305 percentile values of the temperatures, O₃, NO_x, MT and total HOM concentrations for
306 the “non-inversion night” and “inversion night” types. In the non-inversion nights, the
307 air below and above the canopy were relatively well-mixed. The mean and median
308 concentrations of the ground O₃ (21.3 ± 7.7 ppbv and 21.8 ppbv) were close to the tower
309 values (24.9 ± 6.2 ppbv and 23.9 ppbv). The slight difference might be attributed to the
310 higher VOC emissions and larger sink near ground level. In contrast, during the
311 inversion nights, the mean total HOM concentration and O₃ at ground level were
312 generally much lower, only $\sim 33\%$ and $\sim 69\%$ of the tower concentrations, respectively.
313 Instead, the mean and median ground MT concentration (0.70 ± 0.28 ppbv and 0.70
314 ppbv) were ~ 3 times higher than the tower ones (0.24 ± 0.04 ppbv and 0.23 ppbv),
315 respectively. The measured NO_x levels were similar in both types and different heights,



316 though the ambient concentrations were close to the detection limit and therefore small
317 differences might not be observable.

318

319 4.3.2 Case study

320 Two individual nights representing the “non-inversion night” and “inversion night”
321 types were selected and further compared. Figure 5a shows the time series of the
322 meteorological parameters, trace gases and HOMs measured at ground and tower
323 levels of one selected night of “non-inversion night” type (September 11-12, from 21:00
324 to 03:00). A number of measures can be used to assess the local atmospheric stability
325 conditions at a given layer. These measures are commonly based on either the Obukhov
326 length and its associated atmospheric stability parameter or a Richardson number (flux-
327 based, gradient-based, or bulk). Because of its simplicity and the availability of high
328 resolution mean air temperature profiles, the bulk Richardson number (Ri) was used
329 here (Mahrt et al., 2001; Mammarella et al., 2007; Vickers et al., 2012; Alekseychik et
330 al., 2013). It is calculated using:

$$331 \quad Ri = \frac{g\Delta\bar{\theta}\Delta z}{\bar{\theta}(\bar{u})^2} \quad (2)$$

332 where g is the gravitational acceleration, $\Delta\bar{\theta}$ and Δz are the mean potential
333 temperature (10 min averaging interval, same as measurement data) and height
334 difference between the ground and tower levels, respectively, $\bar{\theta}$ and \bar{u} are the mean
335 potential temperature and mean wind velocity at tower level, respectively. During the
336 selected “non-inversion” night, Ri was generally positive but close to 0 (shown in
337 Figure 5a), indicating a weakly stable and relatively well-mixed (i.e. $\Delta\bar{\theta} \rightarrow 0$)
338 condition (Mahrt, 1998; Mammarella et al., 2007). This was also confirmed using the
339 well correlated ground and tower MT and trace gases concentrations.

340



341 **Table 1** Summary of the "Non-inversion night" and "Inversion night" types.

| Type | Non-inversion night | | | | | | Inversion night | | | | | |
|--------|------------------------------------|--------------------------|---------------------------|--------------|--|-----------|--------------------------------------|--------------------------|---------------------------|--------------|-----------|--|
| | September 6, 7, 9, 11, 15, 16, 21* | | | | | | September 5, 8, 10, 12, 13, 14, 19** | | | | | |
| Date | Temperature [°C] | O ₃ [ppbv] | NO _x [ppbv] | MT [ppbv] | Total HOM [10 ⁶ cm ⁻³] | Total HOM | Temperature [°C] | O ₃ [ppbv] | NO _x [ppbv] | MT [ppbv] | Total HOM | |
| Tower | Mean ± 1σ standard deviation | 10.2 ± 2.6 | 24.9 ± 6.2 | 0.50 ± 0.46 | 0.31 ± 0.31 | 2.9 ± 1.9 | 9.5 ± 1.7 | 23.5 ± 2.4 | 0.42 ± 0.26 | 0.24 ± 0.04 | 2.4 ± 0.8 | |
| | Median | 10.9 | 23.9 | 0.38 | 0.17 | 2.8 | 9.2 | 23.3 | 0.34 | 0.23 | 2.3 | |
| | 25% / 75% percentile | 7.9 / 12.4 | 21.3 / 27.4 | 0.16 / 0.67 | 0.15 / 0.24 | 2.2 / 3.2 | 8.1 / 10.9 | 22.0 / 25.3 | 0.22 / 0.54 | 0.21 / 0.26 | 1.8 / 2.8 | |
| Ground | Mean ± 1σ standard deviation | 10.6 ± 2.7 | 21.3 ± 7.7 | 0.43 ± 0.40 | 0.52 ± 0.74 | 1.6 ± 0.6 | 8.3 ± 2.2 | 16.2 ± 6.2 | 0.33 ± 0.24 | 0.70 ± 0.28 | 0.8 ± 0.4 | |
| | Median | 11.5 | 21.8 | 0.31 | 0.22 | 1.7 | 8.5 | 16.8 | 0.27 | 0.70 | 0.7 | |
| | 25% / 75% percentile | 8.1 / 12.8 | 15.8 / 25.9 | 0.15 / 0.53 | 0.21 / 0.31 | 0.9 / 3.2 | 6.6 / 9.9 | 10.8 / 21.8 | 0.17 / 0.44 | 0.46 / 0.82 | 0.5 / 1.2 | |

342 *MT data not available on September 5 and 19.

343 **MT data not available on September 15 and 16.



344 Selected HOM molecules representing the major HOM types (and formation pathways)
345 were summed up and categorized into 4 groups, as shown in Table 2. Each pathway
346 might be influenced differently by boundary layer dynamics and micrometeorological
347 processes. In this study, OH-initiated HOMs were assumed negligible due to the very
348 low OH level in the nocturnal boundary layer.

349

350 **Table 2** Compositions of selected HOM molecules and their main oxidants (Yan et al., 2016).

| | Molecule compositions | Main oxidants | Main terminators |
|-------------------------------|---|-----------------------------------|--------------------------------------|
| CHO_{monomer} | C ₁₀ H ₁₄ O ₇ , C ₁₀ H ₁₄ O ₉ | O ₃ | Self-terminate or RO ₂ |
| CHON_{monomer} | C ₁₀ H ₁₅ O ₉ N ₁ , C ₁₀ H ₁₅ O ₁₁ N ₁ | O ₃ or NO ₃ | NO or Self-terminate/RO ₂ |
| CHO_{dimer} | C ₁₉ H ₂₈ O ₁₁ , C ₂₀ H ₃₀ O ₁₄ | O ₃ | RO ₂ |
| CHON_{dimer} | C ₂₀ H ₃₂ O ₁₂ N ₂ , C ₂₀ H ₃₁ O ₁₃ N ₁ | NO ₃ | RO ₂ |

351

352 All the HOM groups in Figure 5a show stable patterns, and good agreement is observed
353 between the ground and tower measurements in the first half of the night. Variations
354 were observed when air mass change occurred at around 01:00, as indicated by the drop
355 of NO_x concentration and CS, and wind shift (not shown here). However, the HOM
356 groups were still well correlated with each other, suggesting the unchanged well-mixed
357 condition in the non-inversion night.

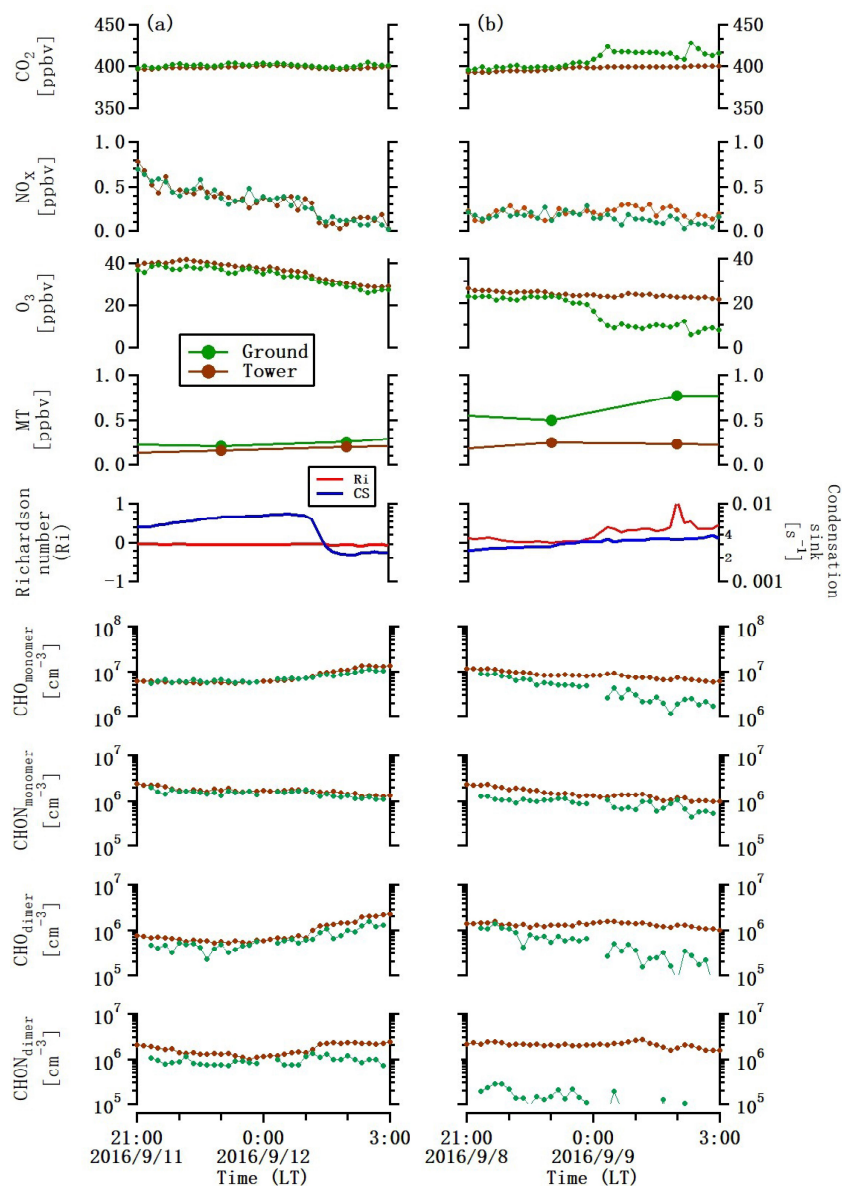
358

359 Figure 5b shows the time series of the trace gases, MT, and HOM groups during an
360 “inversion night” case (September 8-9, from 21:00 to 03:00). *Ri* was generally higher
361 during this night, and increased from ~0.03 (indicating weakly stable condition,
362 Mammarella et al., 2007), at around midnight, to a maximum of ~1.13 (indicating very
363 stable condition) in the remaining night period. Roughly, *Ri* in excess of unity indicate
364 that stably stratified condition appreciably diminish the inverse turbulent Prandtl
365 number (*Pr*) and the efficiency of turbulence to mix heat when compared to momentum



366 (Katul et al., 2014). The parameters measured above the canopy did not show strong *Ri*
 367 fluctuations throughout the night, in contrast, significant variations were observed at
 368 ground level.

369



370

371 Figure 5 (a) Time series of the selected “non-inversion night” case (September 11), and (b) Time series

372 of the selected “inversion night” case (September 8).



373

374 The ground O₃ concentration experienced a rapid decrease at midnight. In about an hour
375 (from 23:30-00:30), ground O₃ concentration dropped by more than half (from 20.1
376 ppbv to 8.6 ppbv), and CO₂ concentration increased as well (from 404 ppbv to 423
377 ppbv). To the contrary, the MT concentration at ground level was almost doubled (from
378 0.49 ppbv to 0.80 ppbv) during the same period. Theoretically, the enhancement of
379 HOM precursor and decrease of oxidant would compensate each other if the sink
380 remained the same, and the ground HOM concentration should also keep constant.
381 However, all the HOM groups showed significant decrease from midnight. In particular,
382 the concentration of the CHO_{monomer} group dropped ~80%, from $8.6 \times 10^6 \text{ cm}^{-3}$ to $1.7 \times$
383 10^6 cm^{-3} , and the concentration of the CHO_{dimer} group decreased from $1.5 \times 10^6 \text{ cm}^{-3}$ to
384 $\sim 1.0 \times 10^5 \text{ cm}^{-3}$. The concentrations of the CHON_{monomer} and CHON_{dimer} groups also
385 experienced large declines (~34% and ~50%, respectively), in the latter half of the night.
386 At 03:00, the CHON_{dimer} concentration was already below the detection limit (1×10^4
387 cm^{-3}). Therefore, the much lower ground HOM concentration might not be totally
388 explained by the change of HOM production, but also some other processes.

389

390 A previous study by Alekseychik et al. (2013) showed that nocturnal decoupled air
391 layers were frequently (with a fraction of 18.6% based on a long-term dataset) observed
392 under high *Ri* condition in the boreal forest. The decoupled layer could strongly
393 influence the ground O₃, MT, and CO₂ concentrations (Rannik et al., 2009, 2012;
394 Alekseychik et al., 2013; Chen et al., 2017), and could also explain the occurrence of
395 the strong temperature inversion during the inversion nights. To explore the possible
396 mechanism resulting in the significant different O₃, MT and HOM concentrations in the
397 sub-canopy level, the mean continuity equation for high Reynolds number flows within
398 the canopy is formulated as (e.g. Katul et al. 2006):

$$399 \quad \frac{\partial \bar{c}}{\partial t} + \bar{U} \frac{\partial \bar{c}}{\partial x} + \bar{W} \frac{\partial \bar{c}}{\partial z} = -S - \frac{\partial \overline{w'c'}}{\partial z} - \frac{\partial \overline{u'c'}}{\partial x} \quad (3)$$

$$400 \quad T_1 + T_2 + T_3 = T_4 + T_5 + T_6 \quad (4)$$



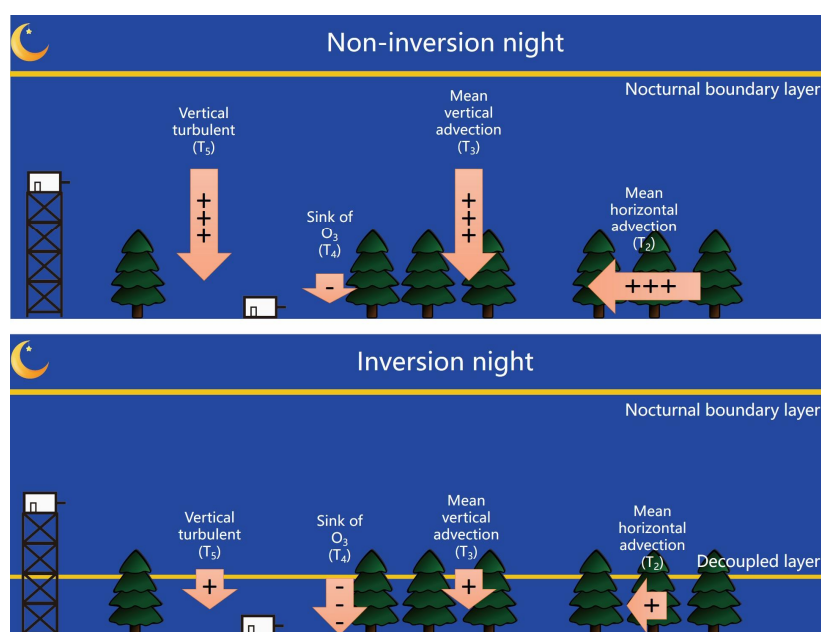
401 where t is time, x and z are the longitudinal and vertical directions, respectively, C
402 is the scalar concentration, U and W are the longitudinal and vertical velocity
403 components, $\overline{w'c'}$ and $\overline{u'c'}$ are the turbulent scalar fluxes in the vertical and
404 horizontal, respectively, and S represents the net sources or sinks (physical, chemical,
405 and biological) of C , and overline represents time averaging over turbulent scales. The
406 6 terms in this equation represent the following (left to right): local rate of change(= T_1),
407 horizontal advection by the mean velocity (= T_2), vertical advection by the mean
408 velocity (= T_3), net sources or sinks (= T_4), net vertical transport by the vertical
409 turbulent flux gradient (= T_5), net horizontal transport by the horizontal turbulent flux
410 gradient (= T_6). Generally, $|T_6| \ll |T_5|$, and is hereafter ignored in the discussion.

411

412 During the non-inversion night, the ground O_3 could be replenished either by vertical
413 turbulent transport (T_5), mean vertical advection from upper boundary layer (T_3), or
414 horizontal advection below canopy (T_2) (as shown in Figure 6). However, for highly
415 stratified flows, T_5 becomes small, as the efficiency of turbulence to transport O_3 to
416 layers near the ground becomes weak (Katul et al., 2014). Vertical and horizontal
417 advection were also small within such a stable layer, and the reduced mean velocity
418 would result in smaller contributions from T_2 and T_3 . Noted that these advective terms
419 tend to be opposite in sign by the virtue of the mean fluid continuity equation (Katul et
420 al., 2006). Instead, the sink of O_3 (T_4) was stronger because of the increasing loss due
421 to a higher surface area-to-volume density (S/V) in this shallow decoupled layer. Under
422 this circumstance, the ground O_3 concentration dramatically decreased when the air
423 layer was forming, and eventually reached a much lower concentration. The decoupled
424 layer also affected the sub-canopy level MT and CO_2 in the inversion night, but resulted
425 in concentration increases as opposed to O_3 . The weakened vertical turbulence (T_5)
426 tended to retain the emissions from ground and understory vegetation within the layer,
427 though T_4 also increased. In general, the increased CO_2 (primary source from the
428 ground) and MT (primary source from the canopy) at ground level are good indicators

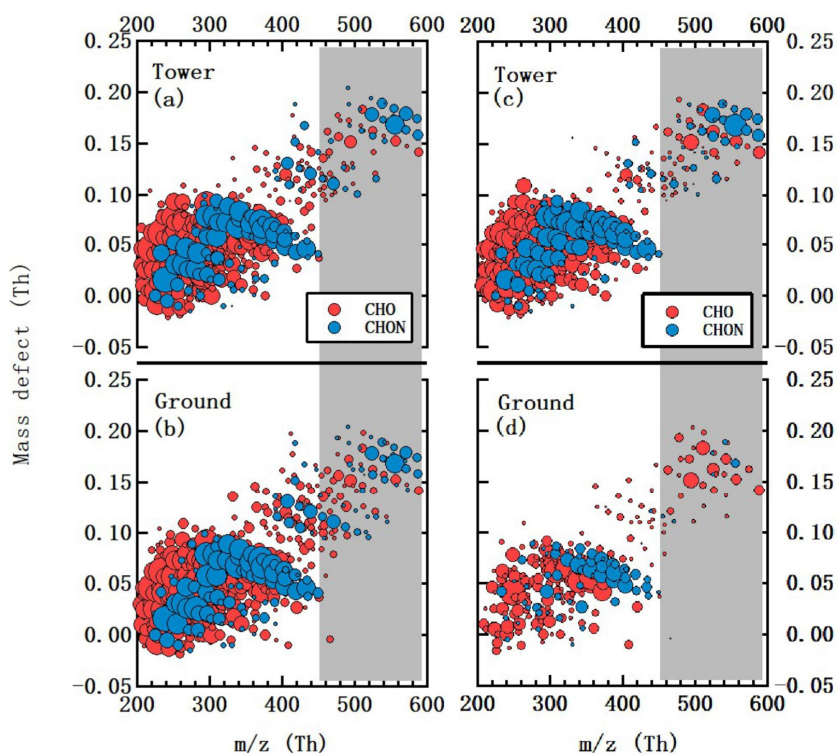


429 for the extent of the mixing in the shallow decoupled layer. At the same time, the strong
430 decrease of O_3 shows how the sinks in this layer are no longer balanced by a large flux
431 of O_3 from upper layers. However, the stabilization of ground-level O_3 concentrations
432 at non-zero values after the initial fast decrease suggests that a small amount of inflow,
433 either via T_3 or T_5 , is still taking place.
434



435
436 Figure 6 Schematic figure showing how vertical mixing, vertical advection, and horizontal
437 advection influence ground O_3 concentrations differently in non-inversion night and inversion night in boreal forest.
438

439 Therefore, the differences between the ground and tower measurements were due to the
440 joint effects of: (i) decoupling between the stably stratified near-ground layer and the
441 canopy top, and the consequent formation of a shallow layer, (ii) weakening of
442 advective and turbulent flux transport terms thereby inhibiting mass exchange between
443 the ground decoupled layer and the remaining nocturnal boundary layer, and (iii)
444 increased surface area to volume within the decoupled layer thereby enhancing T_4 .
445



446

447 Figure 7 Mass defect (MD) plots of the selected “non-inversion night” case (September 11), at (a) tower
448 and (b) ground levels; and “inversion night” case (September 8), at (c) tower and (d) ground levels. The
449 grey shade area denotes the dimer range (m/z 450-600).

450

451 Examination of the selected HOM molecules was useful and efficient to assess the
452 changes in HOMs, however, it might only stand for the major formation pathways.
453 Hence, it was also worthwhile to have a holistic view on the whole mass spectra and all
454 the detected HOMs. The mass defect (MD) plot, with the exact masses of the
455 compounds on the x-axis, the deviation from the integer mass on the y-axis, the
456 compounds plotted in circles and the areas scaled by concentrations, shows the
457 abundance and chemical speciation of all the detected HOMs in the spectra. Figure 7a
458 and 7b are MD plots showing the mean spectra of the selected non-inversion night
459 (September 11) at tower and ground levels. Without the formation of a decoupled layer,



460 nearly identical composition distribution of HOMs were observed. In contrast, during
461 the inversion night (September 8, Figure 7c and 7d), large difference could be found
462 between the two measurement heights. Moreover, a significant fraction of the ground
463 HOMs disappeared in the inversion night, and the concentrations of the remaining
464 HOMs were also lower, confirming the aforementioned results obtained with the
465 selected HOM groups.

466

467 **4.4 Study limitations**

468 Several limitations still existed in this study. The contribution from the potential
469 micrometeorological processes in the layer between 1.5 m and 4.2 m (between the
470 sampling heights of the ground HOMs and other parameters) could not be estimated
471 with the current experiment design (i.e., only two measurement heights). Similarly, the
472 influence from horizontal advection could not be entirely ruled out for the reduced
473 ground-level HOM concentration (and other largely changed species), because of the
474 horizontal inhomogeneity of HOM precursors and oxidants in the sub-canopy level.
475 However, our conclusion was confirmed by the incompatibility between the increasing
476 ground MT and CO₂ concentrations and the advection hypothesis (i.e., all species would
477 show similar tendencies if advection played a major role), indicating the influence of
478 horizontal and vertical advection might be minor when compared to the increasing sink.
479 However, more direct evidence was still needed for further validation, which also
480 highlighted the needs for joint vertical-planar HOM studies.

481

482 **5 Conclusion**

483 Highly oxygenated molecules (HOMs) were measured above the canopy and at ground
484 level (below canopy) in a boreal forest environment during the IBairn campaign,
485 September 2016. Boundary layer dynamics and micrometeorology were found to be



486 important factors that influence the HOMs at ground level, by perturbing both their
487 sources and sinks. In the well-mixed boundary layer (e.g. during daytime or nights
488 without strong inversion), HOM concentrations and other measured species were
489 overall similar between the ground and tower measurements. In contrast, much lower
490 ground level HOM concentrations were observed when nighttime temperature
491 inversion and formation of a decoupled layer occurred in the sub-canopy level. On one
492 hand, the production of the ground-level HOMs could be affected by the decreasing O₃
493 concentrations and the increasing MT concentration in the shallow layer. On the other
494 hand, the surface area to volume ratio dramatically increased in the shallow layer
495 compared to the nocturnal boundary layer. The possibility of losses on surfaces for
496 ground-level HOMs became much larger than usual during inversion nights. The
497 enhanced interaction of air in the decoupled layer with the forest floor was supported
498 by increased concentrations of CO₂, emitted mainly from the ground, in this layer.

499

500 We have presented the first detailed measurements of HOMs below and above the
501 canopy across a wide range of atmospheric stability conditions. The results highlight
502 the significance of near-ground boundary layer dynamics and micrometeorological
503 processes to the ambient HOMs, showing that ground-based HOM measurement might
504 not be representative for the entire nocturnal boundary layer. Conventionally, field
505 measurements of HOMs and other parameters are mostly performed close to ground,
506 and the effect from boundary layer dynamics and micrometeorological processes to the
507 HOM measurements have rarely been considered. Aerosol particle growth and SOA
508 formation rates at ground level are likely to be influenced by the reduced HOM
509 concentrations. Clearly, more vertical and planar measurements of HOMs are needed
510 to confirm the emerging picture presented here. Influence from boundary layer
511 dynamics should be better characterized and evaluated in future field campaigns.

512



513 Acknowledgements

514 This work was supported by the IB AIRN project, the academy of Finland FCoE
515 atmosphere, European commission Actris2 and Actris PPP, the European Research
516 Council (Grant 638703-COALA), transnational access from ENVRI plus, and SMEAR
517 II technical team. Q.Z. thanks ATM-DP (Doctoral Program in Atmospheric Sciences)
518 graduate programs, John Crowley and Max Plank Institute in association with IB AIRN
519 proposal, and the tofTools team for providing tools for mass spectrometry analysis. G.K.
520 acknowledges the support from the U.S. National Science Foundation (NSF-EAR-
521 1344703, NSF-AGS-1644382), the U.S. Department of Energy (DE-SC0011461), and
522 University of Helsinki for supporting a 3-month sabbatical leave at the Division of
523 Atmospheric Sciences.

524

525 Reference:

526 Aalto, P., Hämeri, K., Becker, E., Weber, R., Salm, J., Mäkelä, J. M., Hoell, C., O'dowd,
527 C. D., Hansson, H.-C., Väkevä, M., Koponen, I. K., Buzorius, G. and Kulmala, M.:
528 Physical characterization of aerosol particles during nucleation events, *Tellus B Chem.*
529 *Phys. Meteorol.*, 53(4), 344–358, doi:10.3402/tellusb.v53i4.17127, 2001.
530 Alekseychik, P., Mammarella, I., Launiainen, S., Rannik, Ü. and Vesala, T.: Evolution
531 of the nocturnal decoupled layer in a pine forest canopy, *Agric. For. Meteorol.*, 174, 15–
532 27, doi:10.1016/j.agrformet.2013.01.011, 2013.
533 Bäck, J., Aalto, J., Henriksson, M., Hakola, H., He, Q. and Boy, M.: Chemodiversity of
534 a Scots pine stand and implications for terpene air concentrations, *Biogeosciences*, 9(2),
535 689–702, doi:10.5194/bg-9-689-2012, 2012.
536 Bianchi, F., Tröstl, J., Junninen, H., Frege, C., Henne, S., Hoyle, C. R., Molteni, U.,
537 Herrmann, E., Adamov, A., Bukowiecki, N., Chen, X., Duplissy, J., Gysel, M., Hutterli,
538 M., Kangasluoma, J., Kontkanen, J., Kürten, A., Manninen, H. E., Münch, S., Peräkylä,
539 O., Petäjä, T., Rondo, L., Williamson, C., Weingartner, E., Curtius, J., Worsnop, D. R.,
540 Kulmala, M., Dommen, J. and Baltensperger, U.: New particle formation in the free



541 troposphere: A question of chemistry and timing., *Science*, 352(6289), 1109–12,
542 doi:10.1126/science.aad5456, 2016.

543 Bianchi, F., Garmash, O., He, X., Yan, C., Iyer, S., Rosendahl, I., Xu, Z., Rissanen, M.
544 P., Riva, M., Taipale, R., Sarnela, N., Petäjä, T., Worsnop, D. R., Kulmala, M., Ehn, M.
545 and Junninen, H.: The role of highly oxygenated molecules (HOMs) in determining the
546 composition of ambient ions in the boreal forest, *Atmos. Chem. Phys.*, 17(22), 13819–
547 13831, doi:10.5194/acp-17-13819-2017, 2017.

548 Chen, X., Quéléver, L. L. J., Fung, P. L., Kesti, J., Rissanen, M. P., Bäck, J., Keronen,
549 P., Junninen, H., Petäjä, T., Kerminen, V.-M. and Kulmala, M.: Observations of ozone
550 depletion events in a Finnish boreal forest, *Atmos. Chem. Phys. Discuss.*, 1–24,
551 doi:10.5194/acp-2017-416, 2017.

552 Crouse, J. D., Nielsen, L. B., Jørgensen, S., Kjaergaard, H. G. and Wennberg, P. O.:
553 Autoxidation of Organic Compounds in the Atmosphere, *J. Phys. Chem. Lett.*, 4(20),
554 3513–3520, doi:10.1021/jz4019207, 2013.

555 Eerdekens, G., Yassaa, N., Sinha, V., Aalto, P. P., Aufmhoff, H., Arnold, F., Fiedler, V.,
556 Kulmala, M. and Williams, J.: VOC measurements within a boreal forest during spring
557 2005: on the occurrence of elevated monoterpene concentrations during night time
558 intense particle concentration events, *Atmos. Chem. Phys.*, 9(21), 8331–8350,
559 doi:10.5194/acp-9-8331-2009, 2009.

560 Ehn, M., Junninen, H., Petäjä, T., Kurtén, T., Kerminen, V.-M., Schobesberger, S.,
561 Manninen, H. E., Ortega, I. K., Vehkamäki, H., Kulmala, M. and Worsnop, D. R.:
562 Composition and temporal behavior of ambient ions in the boreal forest, *Atmos. Chem.*
563 *Phys.*, 10(17), 8513–8530, doi:10.5194/acp-10-8513-2010, 2010.

564 Ehn, M., Kleist, E., Junninen, H., Petäjä, T., Lönn, G., Schobesberger, S., Dal Maso,
565 M., Trimborn, A., Kulmala, M., Worsnop, D. R., Wahner, A., Wildt, J. and Mentel, T.
566 F.: Gas phase formation of extremely oxidized pinene reaction products in chamber and
567 ambient air, *Atmos. Chem. Phys.*, 12(11), 5113–5127, doi:10.5194/acp-12-5113-2012,
568 2012.



- 569 Ehn, M., Thornton, J. A., Kleist, E., Sipilä, M., Junninen, H., Pullinen, I., Springer, M.,
570 Rubach, F., Tillmann, R., Lee, B., Lopez-Hilfiker, F., Andres, S., Acir, I.-H., Rissanen,
571 M., Jokinen, T., Schobesberger, S., Kangasluoma, J., Kontkanen, J., Nieminen, T.,
572 Kurtén, T., Nielsen, L. B., Jørgensen, S., Kjaergaard, H. G., Canagaratna, M., Maso, M.
573 D., Berndt, T., Petäjä, T., Wahner, A., Kerminen, V.-M., Kulmala, M., Worsnop, D. R.,
574 Wildt, J. and Mentel, T. F.: A large source of low-volatility secondary organic aerosol,
575 *Nature*, 506(7489), 476–479, doi:10.1038/nature13032, 2014.
- 576 Ehn, M., Berndt, T., Wildt, J. and Mentel, T.: Highly Oxygenated Molecules from
577 Atmospheric Autoxidation of Hydrocarbons: A Prominent Challenge for Chemical
578 Kinetics Studies, *Int. J. Chem. Kinet.*, 49(11), 821–831, doi:10.1002/kin.21130, 2017.
- 579 Hari, P., Nikinmaa, E., Pohja, T., Siivola, E., Bäck, J., Vesala, T. and Kulmala, M.:
580 Station for measuring ecosystem-atmosphere relations: SMEAR, *Phys. Physiol. For.*
581 *Ecol.*, 9789400756, 471–487, doi:10.1007/978-94-007-5603-8_9, 2013.
- 582 Heinritzi, M., Simon, M., Steiner, G., Wagner, A. C., K^{??}rten, A., Hansel, A. and
583 Curtius, J.: Characterization of the mass-dependent transmission efficiency of a CIMS,
584 *Atmos. Meas. Tech.*, 9(4), 1449–1460, doi:10.5194/amt-9-1449-2016, 2016.
- 585 Jokinen, T., Sipilä, M., Junninen, H., Ehn, M., Lönn, G., Hakala, J., Petäjä, T., Mauldin,
586 R. L., Kulmala, M. and Worsnop, D. R.: Atmospheric sulphuric acid and neutral cluster
587 measurements using CI-API-TOF, *Atmos. Chem. Phys.*, 12(9), 4117–4125,
588 doi:10.5194/acp-12-4117-2012, 2012.
- 589 Jokinen, T., Sipilä, M., Richters, S., Kerminen, V.-M., Paasonen, P., Stratmann, F.,
590 Worsnop, D., Kulmala, M., Ehn, M., Herrmann, H. and Berndt, T.: Rapid Autoxidation
591 Forms Highly Oxidized RO₂ Radicals in the Atmosphere, *Angew. Chemie Int. Ed.*,
592 53(52), 14596–14600, doi:10.1002/anie.201408566, 2014a.
- 593 Jokinen, T., Sipilä, M., Richters, S., Kerminen, V.-M., Paasonen, P., Stratmann, F.,
594 Worsnop, D., Kulmala, M., Ehn, M., Herrmann, H. and Berndt, T.: Rapid Autoxidation
595 Forms Highly Oxidized RO₂ Radicals in the Atmosphere, *Angew. Chemie Int. Ed.*,
596 53(52), 14596–14600, doi:10.1002/anie.201408566, 2014b.



597 Jokinen, T., Kausiala, O., Garmash, O., Peräkylä, O., Junninen, H., Schobesberger, S.,
598 Yan, C., Sipilä, M. and Rissanen, M. P.: Production of highly oxidized organic
599 compounds from ozonolysis of β -caryophyllene: laboratory and field measurements,
600 *Boreal Env. Res*, 21, 262–273, 2016.

601 Junninen, H., Ehn, M., Petäjä, T., Luosujärvi, L., Kotiaho, T., Kostianen, R., Rohner,
602 U., Gonin, M., Fuhrer, K., Kulmala, M. and Worsnop, D. R.: A high-resolution mass
603 spectrometer to measure atmospheric ion composition, *Atmos. Meas. Tech.*, 3(4), 1039–
604 1053, doi:10.5194/amt-3-1039-2010, 2010.

605 Katul, G. G., Finnigan, J. J., Poggi, D., Leuning, R. and Belcher, S. E.: The Influence
606 of Hilly Terrain on Canopy-Atmosphere Carbon Dioxide Exchange, *Boundary-Layer
607 Meteorol.*, 118(1), 189–216, doi:10.1007/s10546-005-6436-2, 2006.

608 Katul, G. G., Porporato, A., Shah, S. and Bou-Zeid, E.: Two phenomenological
609 constants explain similarity laws in stably stratified turbulence, *Phys. Rev. E*, 89(2),
610 23007, doi:10.1103/PhysRevE.89.023007, 2014.

611 Kirkby, J., Duplissy, J., Sengupta, K., Frege, C., Gordon, H., Williamson, C., Heinritzi,
612 M., Simon, M., Yan, C., Almeida, J., Tröstl, J., Nieminen, T., Ortega, I. K., Wagner, R.,
613 Adamov, A., Amorim, A., Bernhammer, A.-K., Bianchi, F., Breitenlechner, M., Brilke,
614 S., Chen, X., Craven, J., Dias, A., Ehrhart, S., Flagan, R. C., Franchin, A., Fuchs, C.,
615 Guida, R., Hakala, J., Hoyle, C. R., Jokinen, T., Junninen, H., Kangasluoma, J., Kim,
616 J., Krapf, M., Kürten, A., Laaksonen, A., Lehtipalo, K., Makhmutov, V., Mathot, S.,
617 Molteni, U., Onnela, A., Peräkylä, O., Piel, F., Petäjä, T., Praplan, A. P., Pringle, K.,
618 Rap, A., Richards, N. A. D., Riipinen, I., Rissanen, M. P., Rondo, L., Sarnela, N.,
619 Schobesberger, S., Scott, C. E., Seinfeld, J. H., Sipilä, M., Steiner, G., Stozhkov, Y.,
620 Stratmann, F., Tomé, A., Virtanen, A., Vogel, A. L., Wagner, A. C., Wagner, P. E.,
621 Weingartner, E., Wimmer, D., Winkler, P. M., Ye, P., Zhang, X., Hansel, A., Dommen,
622 J., Donahue, N. M., Worsnop, D. R., Baltensperger, U., Kulmala, M., Carslaw, K. S.
623 and Curtius, J.: Ion-induced nucleation of pure biogenic particles, *Nature*, 533(7604),
624 521–526, doi:10.1038/nature17953, 2016.



- 625 Kulmala, M., Dal Maso, M., Mäkelä, J. M., Pirjola, L., Väkevä, M., Aalto, P.,
626 Miikkulainen, P., Hämeri, K. and O'Dowd, C. D.: On the formation, growth and
627 composition of nucleation mode particles, *Tellus, Ser. B Chem. Phys. Meteorol.*, 53(4),
628 479–490, doi:10.3402/tellusb.v53i4.16622, 2001.
- 629 Kulmala, M., Kontkanen, J., Junninen, H., Lehtipalo, K., Manninen, H. E., Nieminen,
630 T., Petäjä, T., Sipilä, M., Schobesberger, S., Rantala, P., Franchin, A., Jokinen, T.,
631 Järvinen, E., Äijälä, M., Kangasluoma, J., Hakala, J., Aalto, P. P., Paasonen, P., Mikkilä,
632 J., Vanhanen, J., Aalto, J., Hakola, H., Makkonen, U., Ruuskanen, T., Mauldin, R. L.,
633 Duplissy, J., Vehkamäki, H., Bäck, J., Kortelainen, A., Riipinen, I., Kurtén, T., Johnston,
634 M. V., Smith, J. N., Ehn, M., Mentel, T. F., Lehtinen, K. E. J., Laaksonen, A., Kerminen,
635 V.-M. and Worsnop, D. R.: Direct observations of atmospheric aerosol nucleation.,
636 *Science*, 339(6122), 943–6, doi:10.1126/science.1227385, 2013.
- 637 Kürten, A., Bergen, A., Heinritzi, M., Leiminger, M., Lorenz, V., Piel, F., Simon, M.,
638 Sitals, R., Wagner, A. C. and Curtius, J.: Observation of new particle formation and
639 measurement of sulfuric acid, ammonia, amines and highly oxidized organic molecules
640 at a rural site in central Germany, *Atmos. Chem. Phys.*, 16, 12793–12813,
641 doi:10.5194/acp-16-12793-2016, 2016.
- 642 Lauros, J., Nilsson, E. D., Dal Maso, M. and Kulmala, M.: Contribution of mixing in
643 the ABL to new particle formation based on observations, *Atmos. Chem. Phys.*, 7(18),
644 4781–4792, doi:10.5194/acp-7-4781-2007, 2007.
- 645 Mahrt, L.: Nocturnal Boundary-Layer Regimes, *Boundary-Layer Meteorol.*, 88(2),
646 255–278, doi:10.1023/A:1001171313493, 1998.
- 647 Mahrt, L., Vickers, D., Nakamura, R., Soler, M. R., Sun, J., Burns, S. and Lenschow, D.
648 H.: Shallow Drainage Flows, *Boundary-Layer Meteorol.*, 101(2), 243–260,
649 doi:10.1023/A:1019273314378, 2001.
- 650 Mammarella, I., Kolari, P., Rinne, J., Keronen, P., Pumpanen, J. and Vesala, T.:
651 Determining the contribution of vertical advection to the net ecosystem exchange at
652 Hyytiälä forest, Finland, *Tellus B Chem. Phys. Meteorol.*, 59(5), 900–909,



- 653 doi:10.1111/j.1600-0889.2007.00306.x, 2007.
- 654 Mentel, T. F., Springer, M., Ehn, M., Kleist, E., Pullinen, I., Kurtén, T., Rissanen, M.,
655 Wahner, A. and Wildt, J.: Formation of highly oxidized multifunctional compounds:
656 autoxidation of peroxy radicals formed in the ozonolysis of alkenes—deduced from
657 structure–product relationships, *Atmos. Chem. Phys. Discuss.*, 15(2), 2791–2851, 2015.
- 658 Orlando, J. J. and Tyndall, G. S.: Laboratory studies of organic peroxy radical chemistry:
659 an overview with emphasis on recent issues of atmospheric significance, *Chem. Soc.*
660 *Rev.*, 41(19), 6294, doi:10.1039/c2cs35166h, 2012.
- 661 Ouwersloot, H. G., Vilà-Guerau de Arellano, J., Nölscher, A. C., Krol, M. C., Ganzeveld,
662 L. N., Breitenberger, C., Mammarella, I., Williams, J. and Lelieveld, J.:
663 Characterization of a boreal convective boundary layer and its impact on atmospheric
664 chemistry during HUMPPA-COPEC-2010, *Atmos. Chem. Phys.*, 12(19), 9335–9353,
665 doi:10.5194/acp-12-9335-2012, 2012.
- 666 Rannik, Ü., Mammarella, I., Keronen, P. and Vesala, T.: Vertical advection and
667 nocturnal deposition of ozone over a boreal pine forest, *Atmos. Chem. Phys.*, 9(6),
668 2089–2095, doi:10.5194/acp-9-2089-2009, 2009.
- 669 Rannik, Ü., Altimir, N., Mammarella, I., Bäck, J., Rinne, J., Ruuskanen, T. M., Hari, P.,
670 Vesala, T. and Kulmala, M.: Ozone deposition into a boreal forest over a decade of
671 observations: evaluating deposition partitioning and driving variables, *Atmos. Chem.*
672 *Phys.*, 12(24), 12165–12182, doi:10.5194/acp-12-12165-2012, 2012.
- 673 Raupach, M. R. and Thom, A. S.: Turbulence in and above Plant Canopies, *Annu. Rev.*
674 *Fluid Mech.*, 13(1), 97–129, doi:10.1146/annurev.fl.13.010181.000525, 1981.
- 675 Rissanen, M. P., Kurtén, T., Sipilä, M., Thornton, J. A., Kangasluoma, J., Sarnela, N.,
676 Junninen, H., Jørgensen, S., Schallhart, S., Kajos, M. K., Taipale, R., Springer, M.,
677 Mentel, T. F., Ruuskanen, T., Petäjä, T., Worsnop, D. R., Kjaergaard, H. G. and Ehn, M.:
678 The Formation of Highly Oxidized Multifunctional Products in the Ozonolysis of
679 Cyclohexene, *J. Am. Chem. Soc.*, 136(44), 15596–15606, doi:10.1021/ja507146s, 2014.
- 680 Taipale, R., Ruuskanen, T. M., Rinne, J., Kajos, M. K., Hakola, H., Pohja, T. and



- 681 Kulmala, M.: Technical Note: Quantitative long-term measurements of VOC
682 concentrations by PTR-MS – measurement, calibration, and volume
683 mixing ratio calculation methods, *Atmos. Chem. Phys.*, 8(22), 6681–6698,
684 doi:10.5194/acp-8-6681-2008, 2008.
- 685 Tröstl, J., Chuang, W. K., Gordon, H., Heinritzi, M., Yan, C., Molteni, U., Ahlm, L.,
686 Frege, C., Bianchi, F., Wagner, R., Simon, M., Lehtipalo, K., Williamson, C., Craven,
687 J. S., Duplissy, J., Adamov, A., Almeida, J., Bernhammer, A.-K., Breitenlechner, M.,
688 Brilke, S., Dias, A., Ehrhart, S., Flagan, R. C., Franchin, A., Fuchs, C., Guida, R., Gysel,
689 M., Hansel, A., Hoyle, C. R., Jokinen, T., Junninen, H., Kangasluoma, J., Keskinen, H.,
690 Kim, J., Krapf, M., Kürten, A., Laaksonen, A., Lawler, M., Leiminger, M., Mathot, S.,
691 Möhler, O., Nieminen, T., Onnela, A., Petäjä, T., Piel, F. M., Miettinen, P., Rissanen, M.
692 P., Rondo, L., Sarnela, N., Schobesberger, S., Sengupta, K., Sipilä, M., Smith, J. N.,
693 Steiner, G., Tomè, A., Virtanen, A., Wagner, A. C., Weingartner, E., Wimmer, D.,
694 Winkler, P. M., Ye, P., Carslaw, K. S., Curtius, J., Dommen, J., Kirkby, J., Kulmala, M.,
695 Riipinen, I., Worsnop, D. R., Donahue, N. M. and Baltensperger, U.: The role of low-
696 volatility organic compounds in initial particle growth in the atmosphere, *Nature*,
697 533(7604), 527–531, doi:10.1038/nature18271, 2016.
- 698 Vickers, D., Irvine, J., Martin, J. G. and Law, B. E.: Nocturnal subcanopy flow regimes
699 and missing carbon dioxide, *Agric. For. Meteorol.*, 152(1), 101–108,
700 doi:10.1016/j.agrformet.2011.09.004, 2012.
- 701 Viggiano, A. A., Seeley, J. V., Mundis, P. L., Williamson, J. S. and Morris, R. A.: Rate
702 Constants for the Reactions of $XO_3 - (H_2O)_n$ ($X = C, HC, \text{ and } N$) and $NO_3^- (HNO_3)_n$
703 with H_2SO_4 : Implications for Atmospheric Detection of H_2SO_4 , *J. Phys. Chem. A*,
704 101(44), 8275–8278, doi:10.1021/jp971768h, 1997.
- 705 Yan, C., Nie, W., Äijälä, M., Rissanen, M. P., Canagaratna, M. R., Massoli, P., Junninen,
706 H., Jokinen, T., Sarnela, N., Häme, S. A. K., Schobesberger, S., Canonaco, F., Yao, L.,
707 Prévôt, A. S. H., Petäjä, T., Kulmala, M., Sipilä, M., Worsnop, D. R. and Ehn, M.:
708 Source characterization of highly oxidized multifunctional compounds in a boreal



709 forest environment using positive matrix factorization, Atmos. Chem. Phys., 16(19),
710 12715–12731, doi:10.5194/acp-16-12715-2016, 2016.
711 Zhao, J., Ortega, J., Chen, M., McMurry, P. H. and Smith, J. N.: Dependence of particle
712 nucleation and growth on high-molecular-weight gas-phase products during ozonolysis
713 of α -pinene, Atmos. Chem. Phys., 13(15), 7631–7644, doi:10.5194/acp-13-7631-2013,
714 2013.
715